Optics Communications 349 (2015) 180–184

Contents lists available at ScienceDirect

Optics Communications

journal homepage: www.elsevier.com/locate/optcom

Discussion

Optimization of metal-enhanced fluorescence by different concentrations of gold-silica core–shell nanoparticles

Jiawei Chen [a], Kai Wang [a,*], Ke Wu [a], Lihua Qian [a], Hua Long [a], Bing Wang [a], Peixiang Lu [a,b]

[a] School of Physics and Wuhan National Laboratory for Optoelectronics, Huazhong University of Science and Technology, Wuhan 430074, PR China
[b] Laboratory of Optical Information Technology, Wuhan Institute of Technology, Wuhan 430073, PR China

ARTICLE INFO

Article history:
Received 25 December 2014
Received in revised form
13 March 2015
Accepted 17 March 2015
Available online 20 March 2015

Keywords:
Metal-enhanced fluorescence
Core–shell nanoparticle
Absorption and scattering

ABSTRACT

Colloidal solutions of Au/SiO_2 core–shell nanoparticles (NPs) are synthesized. The diameters of Au core are 40 nm, 60 nm, 80 nm and 110 nm and the thickness of SiO_2 shell is 20 nm. The metal-enhanced fluorescence of CdTe quantum dots (QDs) in aqueous solutions is studied by mixing the Au/SiO_2 NPs colloidal solutions with different concentrations. As the molar ratio of the Au/SiO_2 NPs and the CdTe QDs increases, the fluorescence enhancement factor grows rapidly because of the plasmonic enhancement, and then a reduction of the enhancement factor is observed because of the absorption of Au/SiO_2 NPs. The largest fluorescence enhancement factor of 8 is obtained at the optimal molar ratio, when the surface plasmon resonance of the Au/SiO_2 NPs (60 nm) matches the emission peak of the CdTe QDs. The results of our theoretical analysis support the experimental results.

1. Introduction

Noble metal nanoparticles (NPs) have attracted considerable interest as a consequence of a unique optical property called the surface plasmon resonance (SPR) [1–3], which has applications in surface-enhanced Raman scattering [4], high harmonic generation [5], and waveguiding [6]. The SPR effect in noble metal NPs can produce a tremendous near-field enhancement effect below the diffraction limit (hotspots) and shows significant optical enhancement properties [7–9]. In particular, noble metal NPs can also alter the radiative and nonradiative decay rates of nearby fluorophores, resulting in a further enhancement of their fluorescence [10]. Metal-enhanced fluorescence has great value for high resolution imaging [11], single molecule detection [12] and biological labeling [13] applications. However, fluorescence quenching due to the Förster resonance energy transfer (FRET) seriously limits the applications of metal-enhanced fluorescence [14]. As previously reported, many researchers have focused on obtaining a higher fluorescence enhancement factor by optimization noble metal NP geometry [15] and size [16], and of the distance between the fluorophore and the noble metal NPs surface [17]. To the best of our knowledge, the effect of the relative amounts of noble metal NPs with respect to the fluorophores on the metal-enhanced fluorescence has not been addressed to date.

In this letter, colloidal solutions of Au/SiO_2 core–shell NPs are synthesized. The diameters of Au core are 40 nm, 60 nm, 80 nm and 110 nm and the thickness of SiO_2 shell is 20 nm. The resulting metal-enhanced fluorescence is studied as a function of the molar ratios of the Au/SiO_2 NPs and CdTe quantum-dots (QDs) in aqueous solutions. As the molar ratio of the Au/SiO_2 NPs and CdTe QDs increases, the fluorescence enhancement factor grows rapidly because of plasmonic enhancement, and then a reduction of the enhancement factor is observed due to the absorption of Au/SiO_2 NPs, which is a type of long-distance quenching different from FRET. In addition, the size effect of the Au/SiO_2 NPs on the fluorescence enhancement is also studied. When the SPR of the 60 nm Au/SiO_2 NPs matches the emission peak (600 nm) of the CdTe QDs, the highest fluorescence enhancement factor of 8 is obtained. Our theoretical analysis supports the experimental results.

2. Material and method

In the experiments, colloidal solutions of Au NPs with different diameters were synthesized by seed-mediated growth [18]. The morphologies of the Au NPs were observed by transmission electron microscopy (TEM, JEM 2100) are shown in Fig. 1(a)–(d). The diameters of Au NPs are 40 nm, 60 nm, 80 nm and 110 nm, defined by the spherical core size. Tips are synthesized on the Au NPs surface to induce more intensive local fields around the nanoparticles [15]. SiO_2 shell are synthesized to form an 20-nm-thick

* Corresponding author.
E-mail addresses: kale_wong@hust.edu.cn (K. Wang), wangbing@hust.edu.cn (B. Wang).

http://dx.doi.org/10.1016/j.optcom.2015.03.038
0030-4018/

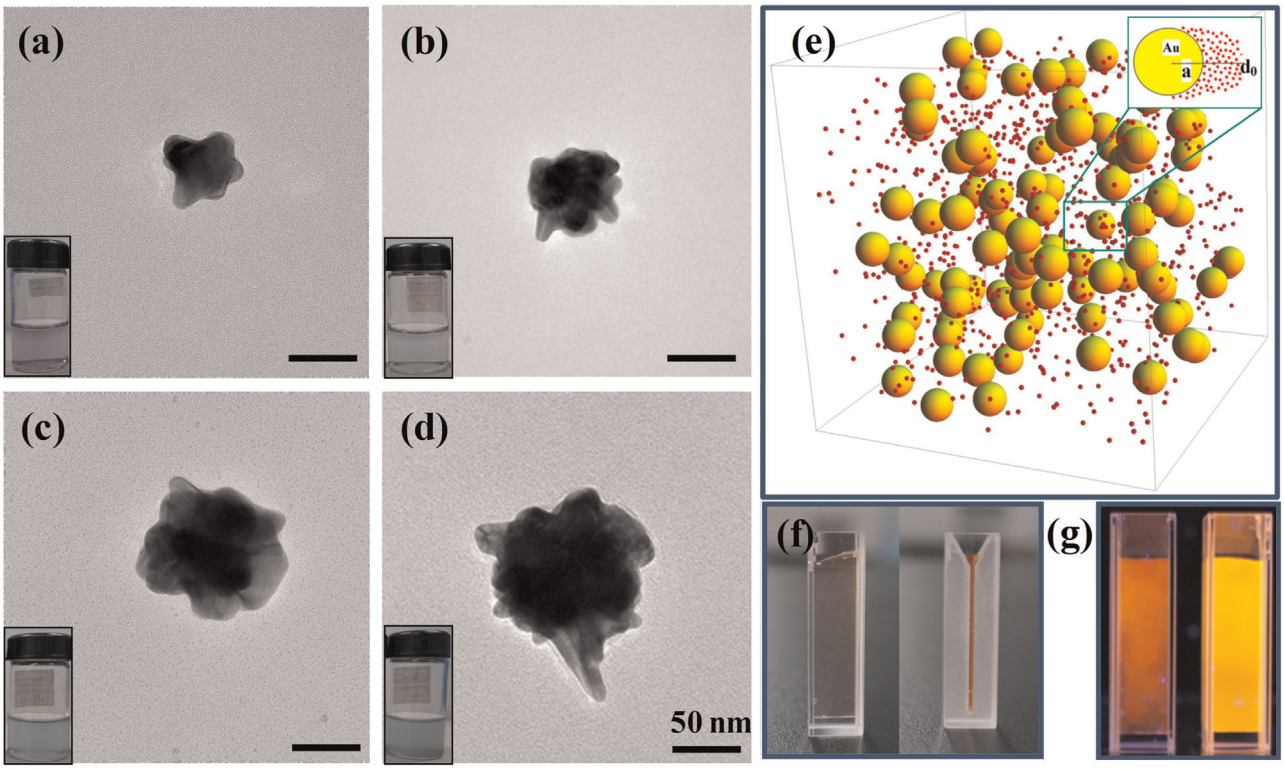

Fig. 1. TEM images of different Au NPs. The diameters are (a) 40 nm, (b) 60 nm, (c) 80 nm, (d) 110 nm. The inset images in (a–d) show the different colors of the Au/SiO_2 NPs colloidal solutions. The scale bar represents 50 nm in each case. (e) An ideal model where the Au/SiO_2 NPs and the CdTe QDs are uniformly distributed in volume *V*. The inset shows the plasmonic enhancement region of an individual Au/SiO_2 NP with an effective work distance of d_0. (f) Front and side images of pure CdTe QD solution in a quartz cuvette. The thickness of the solution is 1 mm. (g) Photoluminescence images of the pure CdTe QD solution (left) and the CdTe QDs and Au/SiO_2 NPs solution mixture (right) under UV light excitation. (For interpretation of the references to color in this figure caption, the reader is referred to the web version of this paper.)

layer to prevent fluorescence quenching induced by non-radiative energy transfer [14]. For the metal-enhanced fluorescence study, the colloidal solutions of the Au/SiO_2 core-shell NPs with various concentrations were mixed into aqueous solutions containing the CdTe QDs. The origin emission efficiency of the CdTe QDs is 40–60% [19]. Fig. 1(e) shows an ideal model for the mixed solution where the Au/SiO_2 NPs and the CdTe QDs are uniformly distributed over a volume *V*. The inset shows that a single NP has an enhancing region with the effective work distance of d_0. Fig. 1(f) shows the front and side images of pure aqueous CdTe QDs solution in a quartz cuvette. Fig. 1(g) shows the pure aqueous CdTe QDs solution (left) and the solution as a mixture of CdTe QDs and Au/SiO_2 NPs (right) under ultraviolet (UV) light excitation. It is clear that the photoluminescence intensity on the right is much stronger than that on the left. In the experiments, the concentration of the CdTe QDs aqueous solution was maintained at a constant 2.1 μM, while the concentrations of the Au/SiO_2 NPs were precisely controlled with respect to this value. These relative ratios shall be discussed further in terms of the molar ratios between the Au/SiO_2 NPs and the CdTe QDs. Samples are uniformly mixed by ultrasonic and all measurements are finished in 2–3 min to prevent any precipitations.

The fluorescence and absorption properties were measured by a fluorescence spectrometer (Jasco, FP-6500) and UV–visible absorption spectroscopy (UV Solutions, U-3310), respectively. Fig. 2(a) shows the measured absorbance and fluorescence emission spectra of the CdTe QDs in the wavelength region from 400 nm to 900 nm. The absorbance peak of the CdTe QDs is located at 455 nm, while the fluorescence emission peak is at 600 nm. The excitation wavelength in experiment was fixed at 455 nm in accordance with the absorbance peak. Fig. 2(b) shows the normalized absorbance of the Au/SiO_2 NPs with Au core diameters of 40 nm, 60 nm, 80 nm and 110 nm, which have SPR peaks located at 574 nm, 611 nm, 656 nm and 686 nm respectively. The SPR peaks show a red shift as the NP diameter increases. Also, the SPR band of Au/SiO_2 NPs (611 nm) matches the CdTe fluorescence band well.

3. Results and discussion

The metal-enhanced fluorescence properties were studied as functions of the molar ratios between the Au/SiO_2 NPs and the CdTe QDs. Because the amount of CdTe QDs used for each measurement was kept constant, the relevant fluorescence enhancement factors can be obtained by dividing the fluorescence intensity of the CdTe QDs and Au/SiO_2 NP solution mixtures by that of the pure CdTe QDs solution. Fig. 2(c) presents fluorescence enhancement factors as functions of the molar ratios between the Au/SiO_2 NPs and the CdTe QDs, for which the SPR peaks of the Au/SiO_2 NPs are located at 574 nm, 611 nm, 656 nm and 686 nm. The fluorescence enhancement factors clearly exhibit similar dependencies on the molar ratios in each case. As the molar ratio increases, the relative amount of the CdTe QDs that enter plasmonic enhancement region of the Au/SiO_2 NPs grows, and thus the relevant fluorescence enhancement factor grows accordingly. As the molar ratio increases further, the fluorescence enhancement factor begins to show a relatively slow reduction process. This fluorescence quenching can be ascribed to the dominant absorption effect caused by superfluous Au/SiO_2 NPs with respect to the number of CdTe QDs. Because the CdTe QDs are not attached to the Au/SiO_2 NPs, the fluorescence quenching due to the absorption is related to a long-distance quenching mechanism that is unlike the short-distance quenching of FRET.

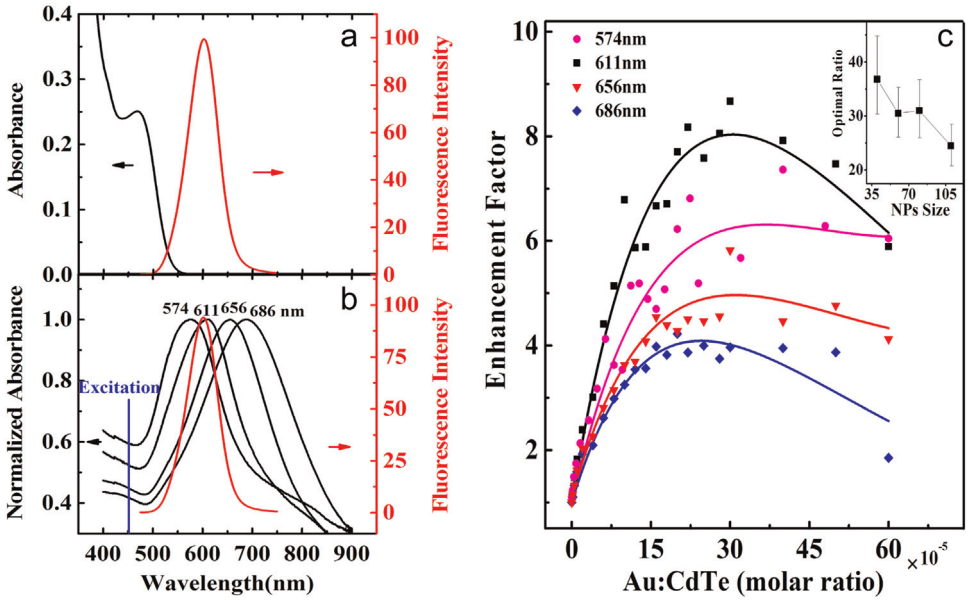

Fig. 2. (a) Absorbance and emission spectra of CdTe QDs. The emission peak is located at 600 nm. (b) Normalized absorbance spectra of the Au/SiO_2 NP colloidal solutions shown in Fig. 1. The red line is the solution emission spectrum of the CdTe QDs in Fig. (a). The blue bar indicates the excitation (455 nm) used in the experiment. (c) Data for the fluorescence enhancement factors as functions of the molar ratio between the Au/SiO_2 NPs and the CdTe QDs. The solid curves indicate the theoretical fittings. The inset shows the optimal molar ratios ($\times 10^{-5}$) for the highest fluorescence enhancement factors, which vary with the size of the Au core NPs. Error bars: the range of the molar ratio corresponding to 1% variation of the maximal fluorescence enhancement factors. (For interpretation of the references to color in this figure caption, the reader is referred to the web version of this paper.)

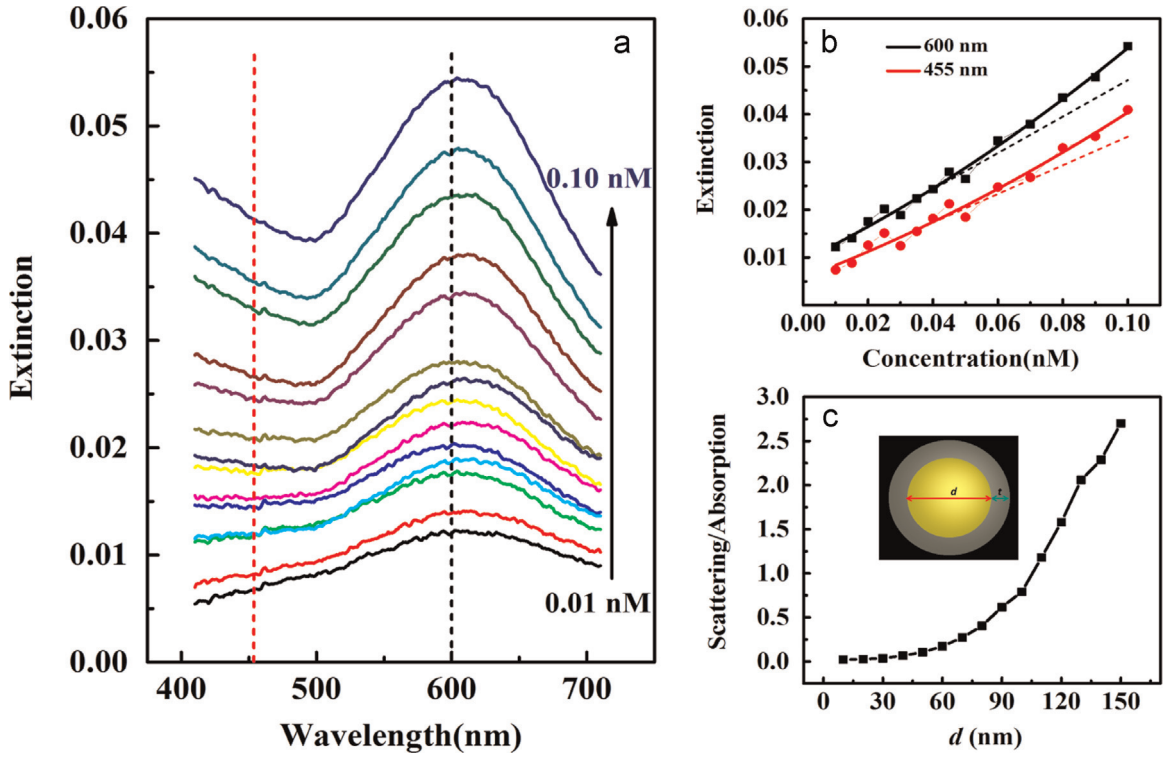

Fig. 3. (a) Measured extinction of Au/SiO_2 NPs (60 nm) at different concentrations. (b) The variation of extinction as concentration at the excitation (455 nm) and CdTe QDs fluorescence (600 nm) wavelength. The solid and dash lines are polynomial and linear fittings respectively. (c) Calculated variation of the ratio of scattering and absorption cross section as the Au core diameter with the SiO_2 thickness keeping at 20 nm for a single spherical Au/SiO_2 nanoparticle. Inset shows the nanoparticle geometry.

A theoretical analysis is performed based on the simple ideal model shown in Fig. 1(e). We consider a solution system with volume V, the radius and the concentration of the Au/SiO_2 NPs are a and C_{Au} respectively. The enhancement effect of the Au/SiO_2 NPs is a function of the distance between the CdTe QDs and the center of the Au/SiO_2 NPs, which is expressed as $E_{(r)}$ [20,21], and the largest effective SPR enhancing distance is d_0. The molar extinction coefficient of Au/SiO_2 NPs is ε and the effective absorption length of the whole solution is L. Then the enhancement factor of the entire system is given by

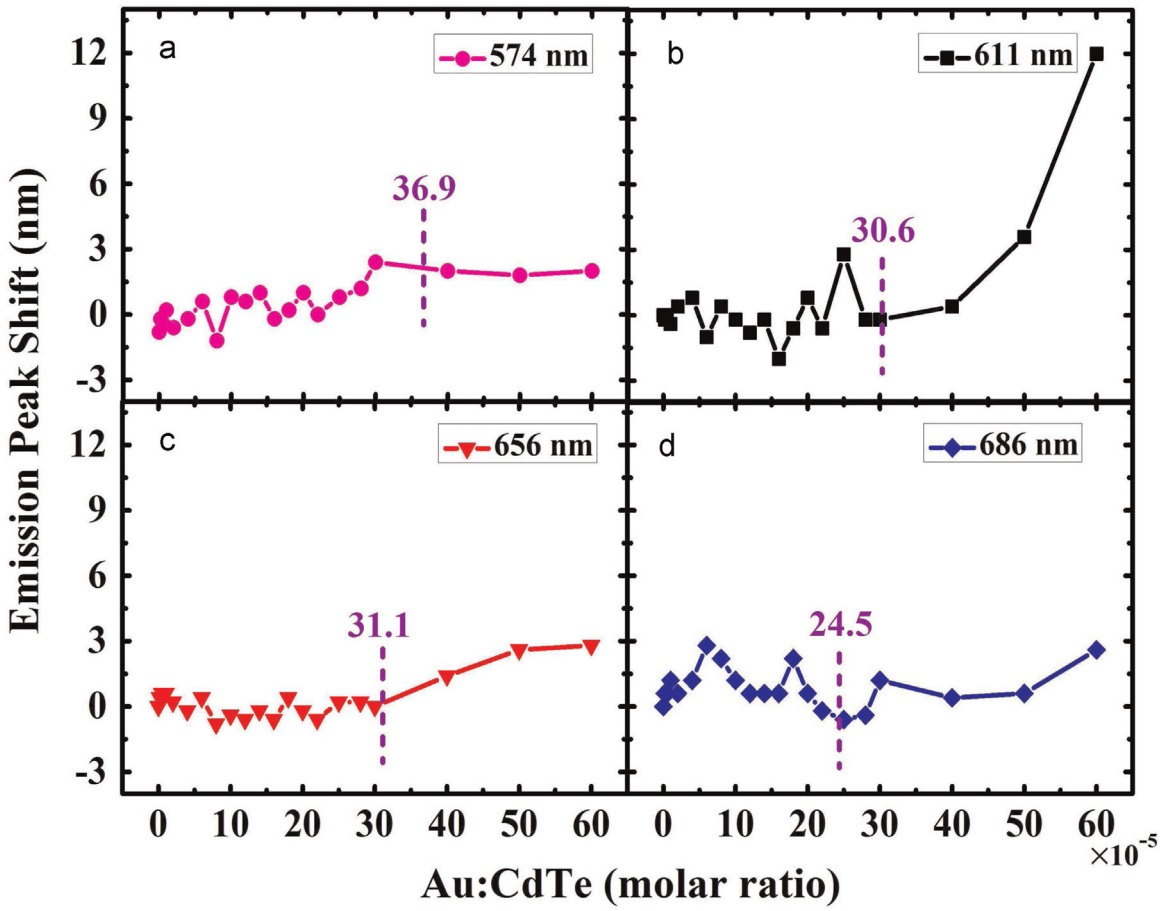

Fig. 4. The red shift of the fluorescence emission spectrum as the increase of the Au/SiO_2:CdTe molar ratio in solution combined CdTe quantum-dots and Au/SiO_2 NPs with absorption of (a) 574 nm, (b) 611 nm, (c) 656 nm and (d) 686 nm. The purple dashes indicate the optimal molar ratios ($\times\ 10^{-5}$) shown in the inset of Fig. 3. (For interpretation of the references to color in this figure caption, the reader is referred to the web version of this paper.)

$$\begin{cases} E = \left[\alpha\left(-1 + \dfrac{1}{1-\beta\cdot C_{Au}}\right) + 1\right]\cdot 10^{-\gamma\cdot C_{Au}} \\ \alpha = \dfrac{\int_a^{d_0}(E_{(r)}-1)\cdot 4\pi r^2\, dr}{\frac{4}{3}\pi a^3} \\ \beta = \dfrac{4}{3}\pi a^3 \\ \gamma = \varepsilon L \end{cases} \quad (1)$$

where α corresponds to the enhancement ability, β corresponds to the size and γ corresponds to the absorption of the Au/SiO_2 NPs. The solid curves shown in Fig. 2(c) indicate the theoretical fitting based on Eq. (1), which supports analysis of the competition between the plasmonic enhancement and the fluorescence quenching due to absorption. In addition, if α, β and γ are accurately known, an optimal Au/SiO_2:CdTe molar ratio can be derived from the derivative of the expression for E in Eq. (1). This will be useful in selecting the optimal ratio of metal NPs and fluorophores in metal-enhanced fluorescence.

In addition, the size effect of the Au/SiO_2 NPs on the fluorescence enhancement factor is also discussed [22,23]. For the four Au/SiO_2 NP sizes shown in Fig. 2(c), the Au/SiO_2 NPs (60 nm) with a SPR peak of 611 nm shows the strongest fluorescence enhancement effect, while the one (110 nm) with a SPR peak at 686 nm appears to be the weakest. This indicates that the strongest fluorescence enhancement effect can be obtained when the SPR band overlaps with the fluorescence emission band. This can be analyzed using a simple quasi-static approximation [20]. For a sphere with a size is much smaller than the wavelength of the light in the surrounding medium, the largest extinction-cross section σ is obtained when the dielectric constants of the metal sphere and the surrounding medium have the following relationship: $Re[\varepsilon_m] = -2\varepsilon_d$. Thus, by considering the enhancement of the radiative decay rate, $E_{(r)} = |1 + 2\left((\varepsilon_m - \varepsilon_d)/(\varepsilon_m + 2\varepsilon_d)\right)(a/r)^3|^2$ [20,21], the strongest radiative decay rate enhancement can be obtained. In the inset of Fig. 2(c), the optimal molar ratios of the solution mixtures containing Au/SiO_2 with core sizes of 40 nm, 60 nm, 80 nm and 110 nm are found to be 36.9, 30.6, 31.1 and 24.5 $\times\ 10^{-5}$ respectively. As the NPs size increases, the optimal molar ratio decreases because the greater volume of the Au/SiO_2 NPs results in more CdTe QDs entering the enhancement region of the Au/SiO_2 NPs.

Scattering should not be ignored in the solution system when the size of Au/SiO_2 NPs exceeds 60 nm [24,25]. In order to judge the influence of scattering of Au/SiO_2 NPs on the fluorescence enhancement results, the extinction of 60 nm Au/SiO_2 NPs at different concentrations have been measured, which is shown in Fig. 3(a). The range of measured concentration is from 0.01 nM to 0.10 nM, including the range of the samples (<0.03 nM) used for enhancing the fluorescence. For the excitation and fluorescence wavelength locating at 455 nm and 600 nm respectively, Fig. 3 (b) shows the variation of extinction as concentration in those two wavelengths. A linear and polynomial fitting is conducted, and the experimental data are off the linear fitting while the polynomial fitting are appropriate. However, if no interactions between the Au/SiO_2 NPs, the scattering and absorption should be proportional

to the nanoparticles concentration, giving rise to the linear variation of extinction. Accordingly, the deviation of linear fitting demonstrates the existence of a multiple scattering when the concentration becomes large. In the range of concentration (<0.03 nM) for enhancing the fluorescence, the extinction can be approximatively regarded as linear variation from the fitting. Thus, weak interaction even no interaction between the Au/SiO_2 NPs is reasonable in low concentration, and calculation of scattering and absorption for single nanoparticle can be conducted to describe the strength of scattering (here expressed as the ratio of scattering cross section and absorption cross section). Theoretical calculated variation of the ratio of scattering and absorption cross section as the Au core diameter for a single spherical Au/SiO_2 nanoparticle is shown in Fig. 3(c), in which the thickness of SiO_2 is kept as 20 nm. The rapid increase of the ratio as the diameter explains the scattering becomes obvious at large nanoparticles. For the nanoparticles used in the experiment with diameters of 40, 60, 80 and 110 nm, the ratios of scattering and absorption cross section are 0.07, 0.17, 0.40 and 1.18 respectively. The low scattering/absorption ratios of 40 nm and 60 nm NPs indicate that scattering effect is limited and the absorption plays a dominant role. For the NPs with Au core of 80 nm and 110 nm, the scattering and absorption effect becomes comparable gradually.

Fig. 4 shows the spectral red-shift of the emission peaks of the solution mixtures compared with that of the pure CdTe QDs solution. No obvious red-shift of the emission peaks can be observed when the molar ratios are lower than the optimal ones of each sample. As the molar ratio increases further, a spectral red-shift is observed in the sample with SPR of 611 nm, as shown in Fig. 4(b). However, the spectral red-shifts are rather weak for the other samples. This is because the SPR wavelength of 611 nm mostly overlaps with the fluorescence emission band of CdTe QDs as shown in Fig. 2(b). The resonance energy transfer [26] between the CdTe QDs and the Au/SiO_2 NPs can be more effective than the others, and leads to the significant spectral red-shift. When the molar ratio is relatively low, the plasmonic enhancement process plays a dominant role and the red-shift related to the fluorescence absorption is weak for each sample. This is further evidence of the competition process of the plasmonic enhancement and the fluorescence quenching caused by the absorption.

4. Conclusion

In conclusion, metal-enhanced fluorescence is studied as a function of molar ratios of Au/SiO_2 NPs and CdTe QDs in aqueous solution with different NPs sizes. As the molar ratio increases, the fluorescence enhancement factor grows rapidly because of plasmonic enhancement, and then a reduction is observed due to the absorption of the Au/SiO_2 NPs, which is related to a long-distance quenching process that is different from FRET. The size effect of the Au/SiO_2 NPs on the fluorescence enhancement is also studied. When the SPR of Au/SiO_2 NPs matches the CdTe QDs emission peak, the highest fluorescence enhancement factor of 8 is obtained. Our theoretical analysis supports our experimental results. The optimized metal-enhanced fluorescence has the potential applications for high resolution imaging, single molecule detection and biological labeling.

Acknowledgements

This work was supported by NSFC (11104095 and 51371084), the Doctoral fund of Ministry of Education of China under Grant no. 20130142110078, and the 973 Program under Grant 2014CB921301.

Appendix A. Supplementary data

Supplementary data associated with this paper can be found in the online version at http://dx.doi.org/10.1016/j.optcom.2015.03.038.

References

[1] E. Hutter, J.H. Fendler, Adv. Mater. 16 (2004) 19.
[2] K.A. Willets, R.P. van Duyne, Ann. Rev. Phys. Chem. 58 (2007) 267.
[3] X.Y. Lang, L.H. Qian, P.F. Guan, J. Zi, M.W. Chen, Appl. Phys. Lett. 98 (2011) 093701.
[4] C.E. Talley, J.B. Jackson, C. Oubre, N.K. Grady, C.W. Hollars, S.M. Lane, T.R. Huser, P. Nordlander, N.J. Halas, Nano Lett. 5 (2005) 1569.
[5] S. Kim, J. Jin, Y.J. Kim, I.Y. Park, Y. Kim, S.W. Kim, Nature 453 (2008) 757.
[6] D. Solis Jr., B. Willingham, S.L. Nauert, L.S. Slaughter, J. Olson, P. Swanglap, A. Paul, W.S. Chang, S. Link, Nano Lett. 12 (2012) 1349.
[7] M. Fu, K. Wang, H. Long, G. Yang, P.X. Lu, F. Hetsch, A.S. Susha, A.L. Rogach, Appl. Phys. Lett. 100 (2012) 063117.
[8] K. Wang, Z. Liu, G.Z. Shen, P.X. Lu, Opt. Express 20 (2012) 24209.
[9] F. Schertz, M. Schmelzeisen, R. Mohammadi, M. Kreiter, H.J. Elmers, G. Schönhense, Nano Lett. 12 (2012) 1885.
[10] M. Fu, L.H. Qian, H. Long, K. Wang, P.X. Lu, Y.P. Rakovich, F. Hetsch, A.S. Sushad, A.L. Rogach, Nanoscale 6 (2014) 9192.
[11] D.R. Larson, W.R. Zipfel, R.M. Williams, S.W. Clark, M.P. Bruchez, F.W. Wise, W.W. Webb, Science 300 (2003) 1434.
[12] A. Kinkhabwala, Z.F. Yu, S.H. Fan, Y. Avlasevich, K. Müllen, W.E. Moerner, Nat. Photon. 3 (2009) 654.
[13] C.J. Lin, T.Y. Yang, C.H. Lee, S.H. Huang, R.A. Sperling, M. Zanella, J.K. Li, J.L. Shen, H.H. Wang, H. Yeh, W.J. Parak, W.H. Chang, ACS Nano 3 (2009) 395.
[14] E. Dulkeith, A.C. Morteani, T. Niedereichholz, T.A. Klar, J. Feldmann, Phys. Rev. Lett. 89 (2002) 203002.
[15] F. Hao, C.L. Nehl, J.H. Hafner, P. Nordlander, Nano Lett. 7 (2007) 729.
[16] F. Tam, G.P. Goodrich, B.R. Johnson, N.J. Halas, Nano Lett. 7 (2007) 496.
[17] Y.Q. Li, L.Y. Guan, H.L. Zhang, J. Chen, S. Lin, Z.Y. Ma, Y.D. Zhao, Anal Chem. 83 (2011) 4103.
[18] F.R. Fan, D.Y. Liu, F.Y. Wu, S. Duan, Z.X. Xie, Z.Y. Jiang, Z.Q. Tian, J. Am. Chem. Soc. 130 (2008) 6949.
[19] A.L. Rogach, T. Franzl, T.A. Klar, J. Feldmann, N. Gaponik, V. Lesnyak, A. Shavel, A. Eychmu1ller, Y.P. Rakovich, J.F. Donegan, J. Phys. Chem. C 111 (2007) 14628.
[20] S.A. Maier, Plasmonics: Fundamentals and Applications, Springer, New York, USA, 2007.
[21] D.V. Guzatov, S.V. Vaschenko, V.V. Stankevich, A.Y. Lunevich, Y.F. Glukhov, S.V. Gaponenko, J. Phys. Chem. C 116 (2012) 10723.
[22] Y. Chen, K. Munechika, D.S. Ginger, Nano Lett. 7 (2007) 690.
[23] O.G. Tovmachenko, C. Graf, D.J. van den Heuvel, A. van Blaaderen, H.C. Gerritsen, Adv. Mater. 18 (2006) 91.
[24] P.K. Jain, K.S. Lee, I.H. El-Sayed, M.A. El-Sayed, J. Phys. Chem. B 110 (2006) 7238.
[25] N.J. Hogan, A.S. Urban, C. Ayala-Orozco, A. Pimpinelli, P. Nordlander, N.J. Halas, Nano Lett. 14 (2014) 4640.
[26] T. Sen, S. Sadhu, A. Patra, Appl. Phys. Lett. 91 (2007) 043104.